RESEARCH ARTICLE

An agrogeophysical modelling framework for the detection of soil compaction spatial variability due to grazing using field-scale electromagnetic induction data

Alejandro Romero-Ruiz[1,2] | Dave O'Leary[3] | Eve Daly[3] | Patrick Tuohy[4] | Alice Milne[1] | Kevin Coleman[1] | Andrew P. Whitmore[1]

[1]Net Zero and Resilient Farming, Rothamsted Research, Harpenden, UK

[2]Department of Agroecology and Environment, Agroscope, Zürich, Switzerland

[3]Hy-Res Research Group, Earth and Life, School of Natural Sciences and Ryan Institute, University of Galway, Galway, Ireland

[4]Animal and Grassland Research and Innovation Centre, Teagasc, Co. Cork, Ireland

Correspondence
Alejandro Romero-Ruiz, Department of Agroecology and Environment, Agroscope, Zürich, Switzerland.
Email: alejandro.romero@agroscope.admin.ch

Present address
Dave O'Leary, Animal and Grassland Research and Innovation Centre, Teagasc, Co. Cork, Ireland

Abstract

Soil compaction is a regarded as a major environmental and economical hazard, degrading soils across the world. Changes in soil properties due to compaction are known to lead to decrease in biomass and increase in greenhouse gas emissions, nutrient leaching and soil erosion. Quantifying adverse impacts of soil compaction and developing strategies for amelioration relies on an understanding of soil compaction extent and temporal variability. The main indicators of soil compaction (i.e., reduction of pore space, increase in bulk density and decrease in soil transport properties) are relatively easy to quantify in laboratory conditions but such traditional point-based methods offer little information on soil compaction extent at the field scale. Recently, geophysical methods have been proposed to provide non-invasive information about soil compaction. In this work, we developed an agrogeophysical modelling framework to help address the challenges of characterizing soil compaction across grazing paddocks using electromagnetic induction (EMI) data. By integrative modelling of grazing, soil compaction, soil processes and EMI resistivity anomalies, we demonstrate how spatial patterns of EMI observations can be linked to management leading to soil compaction and concurrent modifications of soil functions. The model was tested in a dairy farm in the midlands of Ireland that has been grazed for decades and shows clear signatures of grazing-induced compaction. EMI data were collected in the summer of 2021 and autumn of 2022 under dry and wet soil moisture conditions, respectively. For both years, we observed decreases of apparent electrical resistivity at locations that with visible signatures of compaction such as decreased vegetation and water ponding (e.g., near the water troughs and gates). A machine learning algorithm was used to cluster EMI data with three unique cluster signatures assumed to be representative of heavy, moderately, and non-compacted field zones. We conducted 1D process-based simulations corresponding to non-compacted and compacted soils. The modelled EMI signatures agree qualitatively and quantitatively with the

measured EMI data, linking decreased electrical resistivities to zones that were visibly compacted. By providing a theoretical framework based on mechanistic modelling of soil management and compaction, our work may provide a strategy for utilizing EMI data for detection of soil degradation due to compaction.

KEYWORDS

animal treading, agrogeophysics, grazing strategies, hydrogeophysics, soil structure, water dynamics

1 | INTRODUCTION

Soil compaction is an environmental hazard causing soil degradation in croplands and grasslands worldwide. In grasslands, soil compaction is caused largely by livestock treading. Steinfeld et al. (2006) estimated that 20% of the world's grasslands are compacted. Grazing livestock walk over the soil causing soil compaction and poaching (https://www.teagasc.ie/media/website/publications/2017/Segment-002-of-TodaysFarm-Jan-Feb-2017.pdf), which results in a reduction and reorganization of the pore space (especially macroporosity) (Drewry et al., 2008; Tuohy et al., 2015). The impact is greater in wet conditions so the problem is exacerbated in temperate regions (Drewry et al., 2004). Changes in the pore network lead to a dramatic change in the soil's transport properties including hydraulic conductivity, air permeability and gas diffusivity (Or et al., 2021). Such reductions in water and oxygen flow generate anaerobic conditions that limit plant growth and increase nitrous oxide emissions by anaerobic bacterial activity (Pulido-Moncada et al., 2022).

Compaction is a form of soil structure degradation, which is inherently elusive, and difficult to define (Batey, 2009; Benevenute et al., 2020; Bondi et al., 2021; Lipiec, 2000). Properties such as bulk density are insufficient to quantify compaction because similar values of bulk density (or total porosity) may still show wide differences in soil transport properties (Rabot et al., 2018) and other properties may be needed to detect soil compaction such as the soil macroporosity or relative bulk densities (Carter, 1990). Therefore, soil compaction detection and characterization remain very challenging tasks (Keller et al., 2013; Romero-Ruiz et al., 2018). Traditional methods for detecting soil compaction rely on point measurements, soil sampling and time intensive laboratory measurements which makes field-scale quantification of soil compaction particularly difficult, time consuming and costly. In addition, if only few point measurements are made then the spatial variability of soil compaction across a site cannot be characterized. Geophysical methods have recently been proposed to help bridge this scale gap to and allow for field-scale characterization of soil compaction (Romero-Ruiz et al., 2018). They may help delimiting the spatial extent of surface soil compaction (often visible by the naked eye) by livestock trampling and offer additional information about compaction effects in the soil profile.

In particular, geophysical methods that target soil electrical conductivity/resistivity are widely used in soil applications due to their flexibility and the relatively robust understanding of the electrical properties of soils (Friedman, 2005), with electrical resistivity being the inverse of electrical conductivity. Soil compaction signatures captured by electrical properties are known to cause a decrease in electrical resistivity (Seladji et al., 2010), especially in clay soils, potentially due to the better connected soil conductive phase (i.e., surface conductivity) and relatively higher water content resulting from low water mobility in the soil (Romero-Ruiz et al., 2022). Electrical resistivity tomography (ERT) methods are often used to characterize soil compaction (Besson et al., 2013; Keller et al., 2017; Romero-Ruiz et al., 2018). Despite the relative success in detecting and characterizing soil compaction, studies employing the ERT method are still limited in their ability to cover large areas and are usually limited to stationary 2D profiles. More mobile proximal sensing methods, such as electromagnetic induction (EMI), that also measure soil electrical properties offer an alternative means to cover larger areas and can build on the knowledge of how compaction impacts soil electrical properties (Schmäck et al., 2022). In addition, EMI methods have been successfully used to monitor soil texture and layering and related plant development traits (Brogi et al., 2019; von Hebel et al., 2020).

While geophysical methods may be useful at providing information about soil processes and properties, the interpretation of geophysical signatures is not straightforward (Binley et al., 2015). The sensed geophysical properties depend on several factors including soil texture, soil moisture, soil temperature, soil pore connectivity and conductivity of the pore water; disentangling their relative contribution in field measurements is difficult (Friedman, 2005). Coupled modelling of subsurface processes and related geophysical signatures provides a powerful tool for mechanistic interpretation of the measured data, as well as helping to improve survey

ROMERO-RUIZ ET AL.

SoilUse
and Management

BRITISH
SOCIETY
OF SOIL
SCIENCE

WILEY

3 of 16

design for processes and properties of interest (Kowalsky et al., 2004). This framework has been used in agricultural applications to monitor changes in water content and to understand soil plant interactions (Garré et al., 2010, 2011; Kuhl et al., 2018) including those related to soil compaction. Using geophysical methods to support agricultural management by helping to quantify soil compaction may be substantially improved by a coupled mechanistic understanding of (1) the processes causing soil compaction, (2) the impacts of soil compaction on soil properties, (3) related soil processes and (4) the corresponding geophysical signatures. In such a framework, geophysical signatures can be directly linked with compaction and indirectly with land management practices.

Romero-Ruiz et al. (2022) found that the impacts of soil compaction on soil water dynamics may mask its electrical signature; therefore, understanding water dynamics is important. The monitored time (i.e., dry or wet conditions) matters due to changes in water flow and evapotranspiration induced by compaction (Assouline et al., 2014). Despite efforts to model and monitor soil compaction, most studies remain limited to small areas (e.g., focusing on soil profiles) (Keller et al., 2013). There are no modelling studies that link paddock (defined as an area of the farm that is grazed as a single unit) variations in soil compaction with geophysical signatures to the management that induce such compaction. Clustering is the grouping together of spatially coincident, multi-dimensional data that exhibit statistical similarities and the production of a single representative "cluster signature" for each group (Kaufman & Rousseeuw, 2009). Therefore, clustering techniques have the potential to link field-scale (spatial and vertical) variation of EMI data with compaction-induced variations of soil properties and soil's hydrology across a paddock (i.e., compacted zones).

The aim of this work is to develop a modelling framework to demonstrate how EMI data can be used to detect soil compaction in grassland. To achieve this, EMI data were collected from paddocks which have undergone several consecutive years of grazing on a dairy farm in Ireland where detailed land management practices are recorded in the pasturebase system. The collected EMI data are grouped into clusters to provide a single EMI signature for a defined spatial area. A newly developed coupled agro-geophysical modelling approach was then used to interpret grazing-induced compaction in the EMI signatures. The agrogeophysical modelling includes (i) a model of animal movement, (ii) a soil compaction model, (iii) an agro-ecosystem model, (iv) a soil structure-based pedophysical model of soil electrical resistivity and (v) a forward solver for modelling EMI signatures. These modelled EMI signatures are then compared to measured EMI signatures. In Section 2, we describe the acquisition and clustering of EMI data collected on a dairy farm and present the main

features in the data. In Section 3, we present the methodology for detecting and modelling soil compaction with EMI data. Sections 4–6 contain the results, discussion and conclusion, respectively.

2 | METHODS

2.1 | EMI data acquisition and clustering for soil compaction detection

The EMI method uses an oscillating electromagnetic field generated by an alternating electrical current flowing through a transmitter coil (Tx) (Garré et al., 2022). This primary field diffuses into the subsurface and induces so-called eddy currents, whose strength depends on how electrically conductive the medium is. These currents in turn generate a secondary magnetic field, which is then measured by a receiver coil (Rx). The depth of investigation depends on the orientation of the coils (vertical or horizontal coplanar), their separation, the frequency of the Tx coil and the electrical conductivity of the subsurface (Garré et al., 2022). EMI instruments can collect data from multiple depths by either varying the frequency of the Tx coil or by incorporating multiple receiver coils at different separations. In a typical survey, an EMI instrument is carried or towed over the site of interest and data are collected at set time intervals (see Figure 1). Modern instruments can collect data automatically at a high sampling frequency while simultaneously collecting Geospatial Positioning System (GPS) locations. EMI instruments can be attached to a sled behind a quad motorbike and towed over the field (Figure 1a), to collect data consistently over large spatial areas allowing to cover approximately $1\,ha\,h^{-1}$ (see also Figure 1b). A processing flow (i.e., stacking, filtering and interpolation) is then applied to the collected data to correct for GPS offset, reduce noise and obtain a 2D grid of measured apparent electrical conductivities (Figure 1c), for each of the various depths of investigations sensed by the instrument (Figure 1d).

In this study, the geophysical data were collected using the CMD MiniExplorer 6 L (Figure 1a) (https://www.gfinstruments.cz). This instrument has a constant Tx frequency and 6 separate receiver coils, with separations of 0.2, 0.33, 0.5, 0.72, 1.03 and 1.5 m, and coils orientated horizontally resulting in six depth measurements at each spatial position. For each coil separation, the instrument provides an apparent electrical conductivity sensitive to soil depth range (Figure 1d). The instrument was towed ~2 m behind a quad motorbike (Figure 1a) at a speed of approximately $5\,km\,h^{-1}$ and a sampling frequency of 1 Hz. This resulted in an EMI data sample roughly every 1 m in the inline direction. A crossline spacing of ~2 m was maintained throughout the acquisition. A Trimble GNSS system was
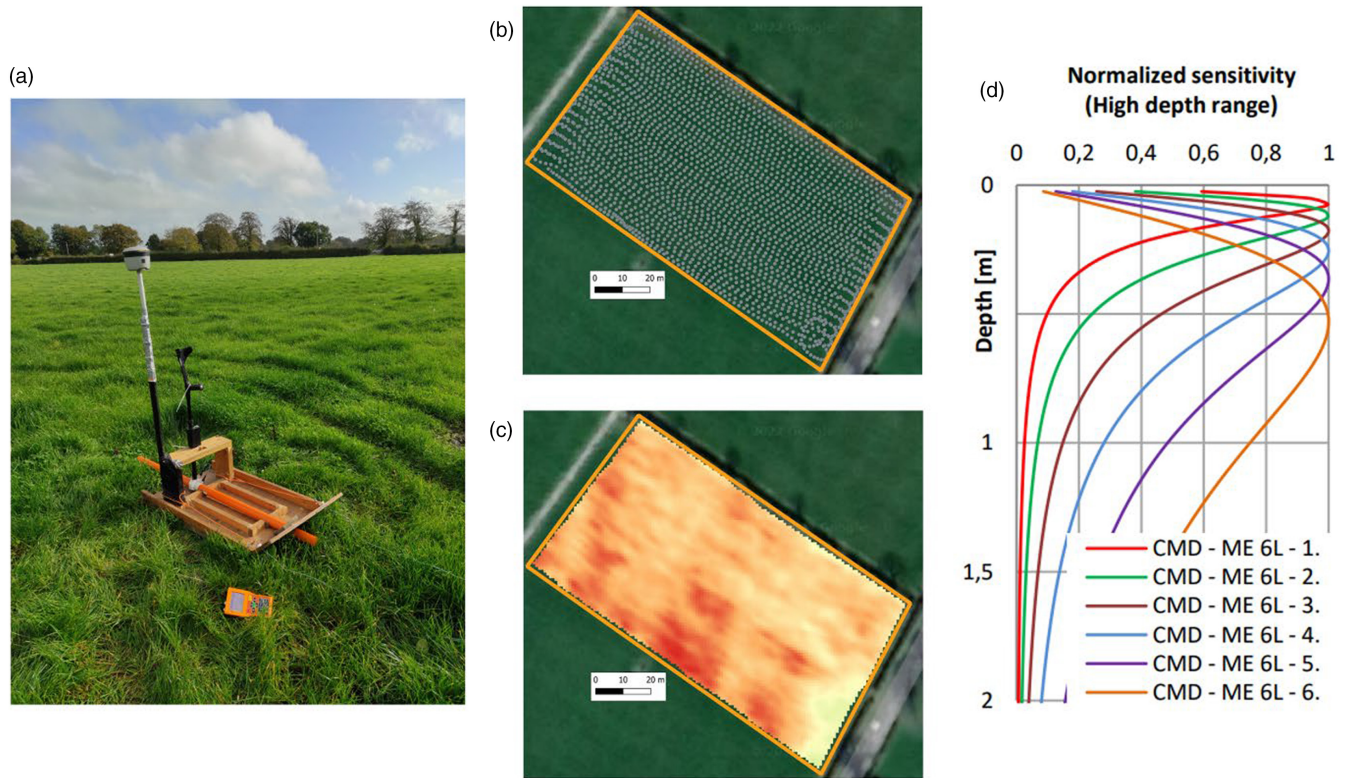
FIGURE 1 (a) Electromagnetic induction (EMI) acquisition system including CMD mini explorer and Trimble global positioning system (GPS) mounted in a purpose-built sledge that is towed by a quad bike. (b) Example of mapped acquisition points measured in a 1 ha paddock at a sampling frequency of 1 Hz. (c) Example of processed EMI data for the acquisition points shown in (b). (d) Normalized sensitivity of EMI data to soil depth as a function of coil separation. The legend endings -1, -2, -3, -4, -5, and -6 correspond to 0.2, 0.33, 0.5, 0.72, 1.03 and 1.5 m coil separations, respectively (from https://www.gfinstruments.cz).

used (models R8 and R2 were used in 2021 and 2022, respectively), providing an accuracy in geographic position of ~1 m. A typical processing flow was applied to each coil separation/depth data layer on a paddock-by-paddock basis. Repeated geographic locations were averaged to remove duplicate readings and corrections were applied to the GPS to account for antenna location relative to instrument centre. A correction was applied to account for the presence of the sled, which was measured prior to each acquisition day. Strong lateral variations ($>1\,\mathrm{mS\,m^{-1}}$) in the data were removed and interpolated and a histogram filter (von Hebel et al., 2014) was applied to remove outliers. Principle component analysis (PCA) filtering was applied (Minsley et al., 2012) to remove high-frequency noise. Finally, each of the six data layers was interpolated using minimum curvature to a $1\,\mathrm{m} \times 1\,\mathrm{m}$ grid. Data from the 0.2-m dipole separation were discarded because they showed high noise levels, due to the presence of air beneath the sled. EMI data often need to be calibrated due to instrument drift. Here, calibration coefficients were generated from a single coincident EMI and ERT calibration line. The coefficients were calculated for each coil separation using EM4SOIL (software for Electromagnetic Tomography. http://www.emtomo.com/) and applied to

the cluster centres to improve matching to modelled EMI for the times presented. The data are then converted to apparent electrical resistivity (ρ_a), which is the inverse of the apparent electrical conductivity, to match the outputs from the modelling section (Section 2.2.3). Additionally, the relative apparent resistivity ($\overline{\rho_\mathrm{a}}$) is calculated as:

$$\overline{\rho_\mathrm{a}} = \frac{\rho_{\mathrm{a}_i} - \rho_{\mathrm{a}_\mathrm{mean}}}{\rho_{\mathrm{a}_\mathrm{mean}}}, \tag{1}$$

where ρ_{a_i} is the apparent resistivity measured at any given location in the paddock and $\rho_{\mathrm{a}_\mathrm{mean}}$ is the mean apparent electrical resistivity of the paddock.

This study uses an unsupervised machine learning technique called self-organizing maps (Kohonen, 2013) to detect zones with a similar EMI signature. Typically, a range of appropriate number of clusters for a given data set is determined using a set of stability metrics (e.g., the MCASD; O'Leary et al., 2023). In this study, this method is applied independently for each paddock and time, considering data from all available EMI coil separations (i.e., sensitive to different soil depth ranges, Figure 1d). By doing this, the zonation accounts for soil compaction effects in the apparent electrical resistivity due to (a) shallow

variations of soil bulk properties and (b) variations in the soil moisture dynamics in the soil profile.

2.2 | Soil compaction explicit agrogeophysical modelling

Grazing management was linked to measured geophysical signatures by developing an explicit soil compaction agrogeophysical modelling framework that couples: (i) an animal movement model (Section 2.2.1), (ii) a soil compaction model (Section 2.2.2), (iii) an agroecosystem model (Section 2.2.3), (iv) a pedophysical model of electrical properties (Section 2.2.4) and (v) a forward solver for simulating EMI data (Section 2.2.5). The modelling scheme is shown in Figure 2.
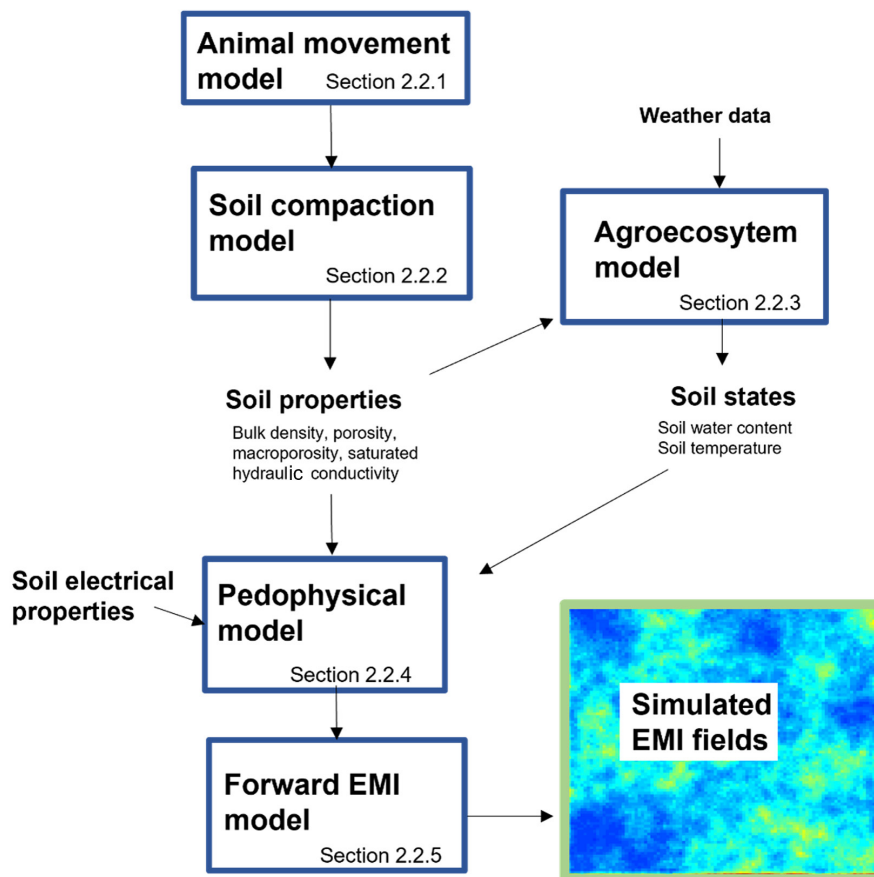
2.2.1 | Animal movement model

The model by Romero-Ruiz, Milne, et al. (2023) was used for representing animal movement as random walks (see also Rivero et al., 2021; Stephenson & Bailey, 2017). The model describes animal movement in polar coordinates characterized by two main properties: rotation angle and travelling distance that indicate the direction to which

animals will move and the Euclidean distance between the current and next location. Animal movement patterns are then obtained by sequentially sampling from probability density functions (PDF) that are representative of the rotation angle and travelling distance to update the position of the targeted animal. A uniform PDF is used to sample rotation angles from 0 to 2π and the travelling distance is sampled from a Weibull distribution given by:

$$p_w = f_w(x_w; a_w, b_w) = \begin{cases} \dfrac{b_w}{a_w}\left(\dfrac{x_w}{a_w}\right)^{b_w-1} e^{(x_w/a_w)^{b_w}} & \text{if } x \geq 0, \\ 0 & \text{if } x < 0, \end{cases}$$ (2)

where p_w is the probability of the travelling distance x_w, and a_w and b_w are the Weibull parameters that are used to scale the travelling distance and highlight the distances with highest probability. Animal movement is then simulated for each grazing day. For this, an area in which animals will move is defined and discretized into $1\,\text{m} \times 1\,\text{m}$ grid cells. Animal spatial locations within such area are then sampled using the model described above using a given number of steps per day (N_d). A heat map of animal movement is finally obtained by calculating the number of times in which animals were located in a given grid cell.

FIGURE 2 Flow chart of the coupled agrogeophysical modelling framework used in this work. It includes a model of animal movement that simulates grazing management, a soil compaction model that predicts soil structure dynamics, an agroecosystem model for soil process modelling, a pedophysical model of electrical properties and a forward model of electromagnetic induction (EMI) data. The section of the manuscript in which each model is described is provided in each block.

2.2.2 | Soil compaction model

Once animal movement and statistics about compaction locations are obtained (Section 2.2.1), a soil compaction model (Romero-Ruiz, Monaghan, et al., 2023) was used to systematically calculate the corresponding temporal dynamics of soil bulk density (d), macroporosity (w_{mac}) and saturated hydraulic conductivity (K_{sat}). In such a model, the soil is conceptualized as a dual-domain porous media formed by (1) a soil matrix that is represented as an assembly of soil aggregates presenting intra-aggregate porosity and (2) a soil macroporous region that can be conceptualized as inter-aggregate porosity. The model used the rheology models proposed by Ghezzehei and Or (2001) based on Bingham's theory and simulates the lasting effect of one treading. Each event produces an irreversible deformation, ϵ_v, which is modelled using information about the initial (prior to compaction) strain ϵ_0, the axial load and duration of stress application and the soil rheological properties as:

$$\epsilon_v(t) = \left[\epsilon_B^2 S_{sm}(t)^{N_v}(1-\cos(\omega t)) + \epsilon_0^2\right]^{\frac{1}{2}}, \quad (3)$$

where t is the time, ω is the angular frequency, ϵ_B comprises information of the soil rheological properties and the characteristics of the compaction event (e.g., weight of animal and walking speed), $S_{sm} = \theta_{sm}/\phi_{sm}$ is the water saturation in the soil matrix, where θ_{sm} is the water content in the soil matrix and N_v is an empirical exponent. The compaction-induced strain is then used to calculate d, w_{mac} and K_{sat}. Further details on the soil compaction model and limitations can be found in Romero-Ruiz, Monaghan, et al., (2023).

The soil compaction model can also estimate recovery of soil properties as a function of time once the compacting elements are removed. Soil macro, meso and microporosities change dynamically as a function of time and recovery is expected to be associated with biological activity, climatic cycles and management. Meurer et al. (2020) showed that macroporosity (w_{mac}) recovers at an exponential rate asymptotically to a maximum macroporosity (w_{mac_0}). Similarly, soil structure recovery in the viscous strain can be modelled as:

$$\epsilon_v = \epsilon_0 - (\epsilon_0 - \epsilon_i)e^{-d_r/\lambda_{tr}}, \quad (4)$$

where ϵ_{mac_i} is the soil strain, representing the strain resulting after the grazing season, d_r is the number of days after the last grazing season, and λ_{tr} determines the recovery rate.

2.2.3 | Agroecosystem modelling

The compaction-induced dynamics of soil properties derived from the compaction model (Section 2.2.2) are entered into an agroecosystem model to explicitly account for compaction-induced soil degradation in important soil processes such as water flow, plant growth, nutrient and carbon cycling. The Rothamsted Landscape Model (RLM) (Coleman et al., 2017) was used in this study. The RLM incorporates daily updates of key soil properties affected by compaction during the grazing days. As illustrated in Figure 2, the RLM outputs water content and temperature, which are the controlling factors for electrical properties of the soil sensed by the EMI method. The RLM discretized the soil in three layers with model-defined interfaces at 0.23 and 0.46 m (final layer ends at 1 m). To include soil structure effects in soil functioning, a slightly modified version of the RLM was used. In such version, the water retention and hydraulic properties are modelled using the dual domain approach by Durner (1994) as:

$$S_e = \frac{\theta-\theta_r}{\phi_T-\theta_r} = w_{sm}\left[1+(\alpha_{sm}h)^{n_{sm}}\right]^{1-\frac{1}{n_{sm}}} + w_{mac}\left[1+(\alpha_{mac}h)^{n_{mac}}\right]^{1-\frac{1}{n_{mac}}}, \quad (5)$$

and

$$K_{soil} = r_k K_{sm} \frac{\left(w_{sm}S_{e_{sm}}+w_{mac}S_{e_{mac}}\right)^{0.5}}{\left(w_{sm}\alpha_{sm}+w_{mac}\alpha_{mac}\right)^2} \left(w_{sm}\alpha_{sm}\left[1-\left(1-S_{e_{sm}}^{\frac{n_{sm}}{n_{sm}-1}}\right)^{1-\frac{1}{n_{sm}}}\right]+w_{mac}\alpha_{mac}\left[1-\left(1-S_{e_{mac}}^{\frac{n_{mac}}{n_{mac}-1}}\right)^{1-\frac{1}{n_{mac}}}\right]\right)^2, \quad (6)$$

where h is the pressure head, S_e is the effective saturation of the soil, θ_r is the residual water content, n_i is the van Genuchten exponent (relating to soil texture) and α_i is related to the inverse of the air-entry pressure. The saturated hydraulic conductivity of the soil $K_{sat} = r_k K_{sm}$ is defined as the product of the saturated hydraulic conductivity of the soil matrix K_{sm} and the ratio $r_k = K_{sat}/K_{sm}$ which is a function of the soil macroporosity.

2.2.4 | Pedophysical modelling of electrical properties

Translating the simulated soil states to soil electrical properties requires a pedophysical model linking the soil water content, temperature, porosity and texture to the soil electrical resistivity. There are a multitude of predictive (or forward) models for predicting the soil electrical resistivity that often consider the main mechanism of electrical conduction in soils through the solid and liquid phases (Bussian, 1983; Linde et al., 2006; Waxman & Smits, 1968). To be consistent with the soil compaction model (Section 2.2.2), a dual-domain electrical model was used. This model is based on differential effective

media (Sen et al., 1981) and represents the soil as a combination of a soil matrix and a macroporous space. The electrical conductivity of the soil (σ_{soil}) is expressed as (Romero-Ruiz et al., 2022):

$$\sigma_{soil} = (1 - w_{mac})\sigma_{sm}\left(\frac{1 - \sigma_{mac}/\sigma_{sm}}{1 - \sigma_{mac}/\sigma_{soil}}\right)^{M_{soil}}, \quad (7)$$

where σ_{mac} and σ_{sm} are the electrical conductivity of the macroporous region and the soil matrix, respectively; and M_{soil} is an exponent that is understood to be related to the connectivity of soil aggregates and thus may be used to indicate compaction (Romero-Ruiz et al., 2022). The conductivity of the soil matrix σ_{sm} depends on the surface conductivity σ_s and the electrical conductivity of the pore fluid σ_f. Full expressions for σ_s and σ_f can be found in Romero-Ruiz et al. (2022). In this work, the electrical resistivity of the soil is reported, which is the reciprocal of the soil electrical conductivity:

$$\rho_{soil} = 1/\sigma_{soil}. \quad (8)$$

A temperature correction model is applied to the electrical resistivity to account for temperature effects using the model by Campbell et al. (1948).

2.2.5 | Forward modelling of EMI data

The EMagPy forward model, developed by McLachlan et al. (2021), was used to convert the predicted true electrical resistivity to apparent resistivity, which is what is measured by EMI instruments. This allows a comparison between modelled results and acquired EMI data. EMagPy is a 1D open-source modelling tool that can be used with python scripts or in graphical user interface (GUI). It offers the flexibility of forward modelling of EMI data for different coil separations.

3 | CASE STUDY: DAIRY FARM IN TIPPERARY, IRELAND

3.1 | Study site and grazing history

The field site used in this study is a working dairy farm located in County Tipperary, Ireland (Figure 3a). This dairy farm is made up of several paddocks with a total spatial extent of ≈50ha. It is located ≈100m above mean sea level, and its annual precipitation averages 980mm (https://www.teagasc.ie/crops/grassland/heavy-soils/). Cattle are housed when ground conditions are poor; otherwise, they graze in paddocks, typically from February to November. Poor conditions are most likely to occur when there have been consecutive days of rain.

We did not perform soil sampling campaigns for this study. In order to infer soil compaction, we relied instead in pasture base information, pasture records, visual assessment of the studied farm and extensive literature reports of soil compaction in grazed pastures. Soil compaction has been consistently observed for grazed pastures (such as the
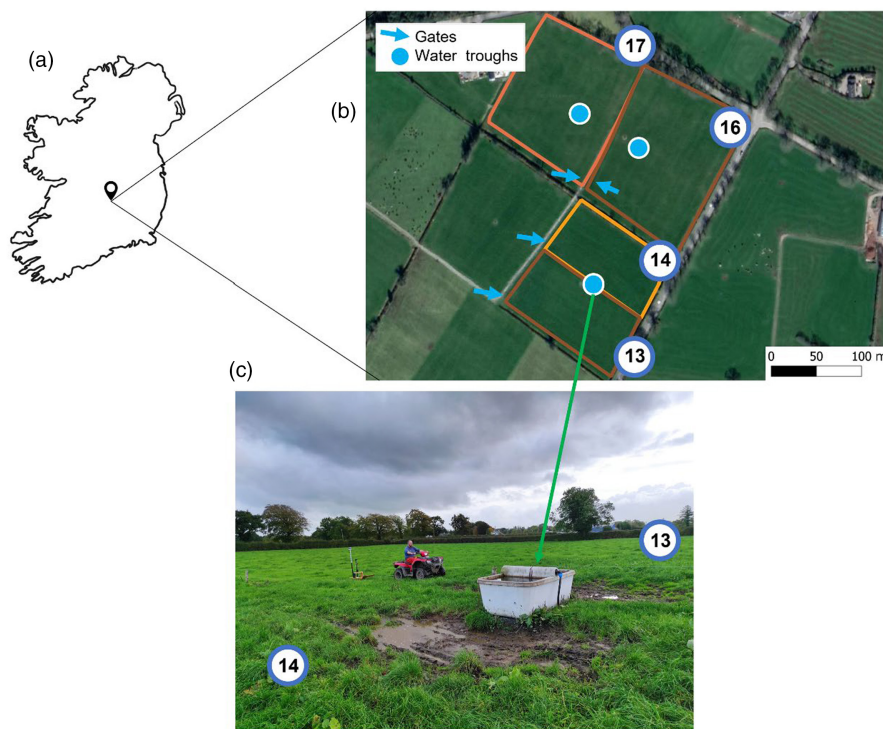
FIGURE 3 (a) The location of the study site in County Tipperary, Ireland. (b) An aerial photograph of paddocks 13, 14, 16 and 17. The locations of the paddock gates and water troughs are highlighted. (c) A photograph of paddocks 14 and 13 where compacted areas can be seen around the water trough.

one used in this study) across the world (Hu et al., 2021). This is typically concentrated around spatial locations that experience highest trampling frequency (e.g., near water troughs, entry gates, shelter) (Rivero et al., 2021). As expected, we observed poaching, water ponding and reduced vegetation, which are common signs of soil compaction, near the entry gates and water troughs of all monitored paddocks (Figure 2c, see more pictures in the Figure S1).

EMI data were acquired from four paddocks on this farm, paddocks 13, 14, 16 and 17 with respective areas of 1.01, 0.91, 2.05 and 1.87 ha. These paddocks have been grazed by a herd of dairy cows an average of 8 days per year per paddock in the period between 2014 and 2023. The herd is composed by 124 cows since 2019. According to in situ single point measurements in each paddock, the soil type of all paddocks is typical surface-water gley under the Irish soil classification "Great Group" level (Creamer & O'Sullivan, 2018). In a second point measurement at the north half of paddock 16, the soil was classed as a "Brown Earth" (see Figure S2).

The EMI data were collected over two separate acquisition campaigns. A full survey of the farm took place in the summer of 2021, with paddocks 13 and 14 being acquired on 16 July 2021 (Time 1) and paddocks 16 and 17 being acquired on 3 September 2021 (Time 2). These four paddocks were revisited on 20 October 2022 (Time 3) specifically for this study to include different soil moisture conditions. Environmental variables (i.e., temperature, rainfall and solar radiation) recorded on this farm were used to predict the soil moisture deficit (SMD) (Schulte et al., 2005). This shows that data for this study were acquired under dry (Times 1 and 2) and wet (Time 3) soil conditions. Data were processed and clustered (see Section 2.1) independently for each paddock/acquisition date.

3.2 | Application of agrogeophysical modelling framework

In this study, modelled electrical signatures of compacted and non-compacted soil in EMI data were compared. It is assumed that compacted areas were trampled a given number of steps per grazing day (i.e., $N=17$) and non-compacted were not trampled at all. The starting conditions within the soil model were selected based on published values of physical and electrical properties of soils with similar textures. The initial property values were set to $d=1.29\,\mathrm{g\,cm^{-2}}$, $w_{\mathrm{mac}}=0.15\,\mathrm{cm^3cm^{-3}}$ and $K_{\mathrm{sat}}=195\,\mathrm{cm\,h^{-1}}$ (Hu et al., 2021). The water retention properties were selected based on soil with similar textures as reports by Carsel and Parrish (1988) to $\alpha_{\mathrm{sm}}=0.04\,\mathrm{cm^{-1}}$, $n_{\mathrm{sm}}=1.9$, $\theta_{r_{\mathrm{sm}}}=0.06\,\mathrm{cm^3\,cm^{-3}}$, and $K_{\mathrm{sm}}=1.9\,\mathrm{cm\,h^{-1}}$. These

properties were also assigned all three layers of the RLM (Figure 2).

To generate a compacted soil scenario, true recorded information about grazing days and trampling amount was used to calculate changes in soil physical and electrical properties. For simplicity, only compaction-induced changes in the soil bulk density, soil macroporosity and the saturated hydraulic conductivity were allowed to be varied by the model. Similarly, compaction only induces changes in one key pedophysical parameters: soil macroporosity. The rest of the pedophysical parameters were the same for both compacted and non-compacted soil scenarios. Soil structure recovery was modelled using a recovery rate of $\lambda_{\mathrm{tr}}=100\,\mathrm{days}$, in agreement with recovery rates observed by Drewry (2006). Here, we do not model changes in M_{soil} due to compaction and rather use values of $M_{\mathrm{soil}}=5$ for both compacted and non-compacted soils. The electrical conductivity of water was set to $\sigma_{\mathrm{w}}=0.04\,\mathrm{S\,m^{-1}}$ (Farahani et al., 2018). The soil surface conductivity (σ_{s}), known to be highly variable, was used as a calibration variable. The simulated apparent electrical resistivities were calibrated to the cluster centre data corresponding to low-compacted paddock 13 at Time 1 using a grid search.

4 | RESULTS

4.1 | Observed EMI data

Figure 4 shows maps of relative apparent resistivity ($\overline{\rho_{\mathrm{a}}}$) corresponding to a coil separation of 0.33 m (shallowest reading with highest sensitivity to detect compaction) together with SMD calculations for 2021 and 2022. The SMD corresponding to Times 1 and 2 is similar (~40) and higher than the SMD for Time 3 (~−10), suggesting dry conditions for Times 1 and 2 and wet conditions for Time 3. Thus, higher absolute values of apparent electrical resistivities were measured at Time 1 and Time 2 (dry conditions).

4.2 | Relative apparent resistivity of in-field EMI survey

The relative apparent resistivities (Figure 4a–c) are paddock independent, meaning that they were calculated as the relative change with respect to the mean value of apparent resistivity of soil collected for each paddock/acquisition date. This allowed comparison of data collected in different years. For all paddocks/acquisition date, the range in the relative apparent resistivity $\overline{\rho_{\mathrm{a}}}$ remains stable, with most values falling between −60% and +60% of relevant mean value. This indicates that, for these soils, spatial
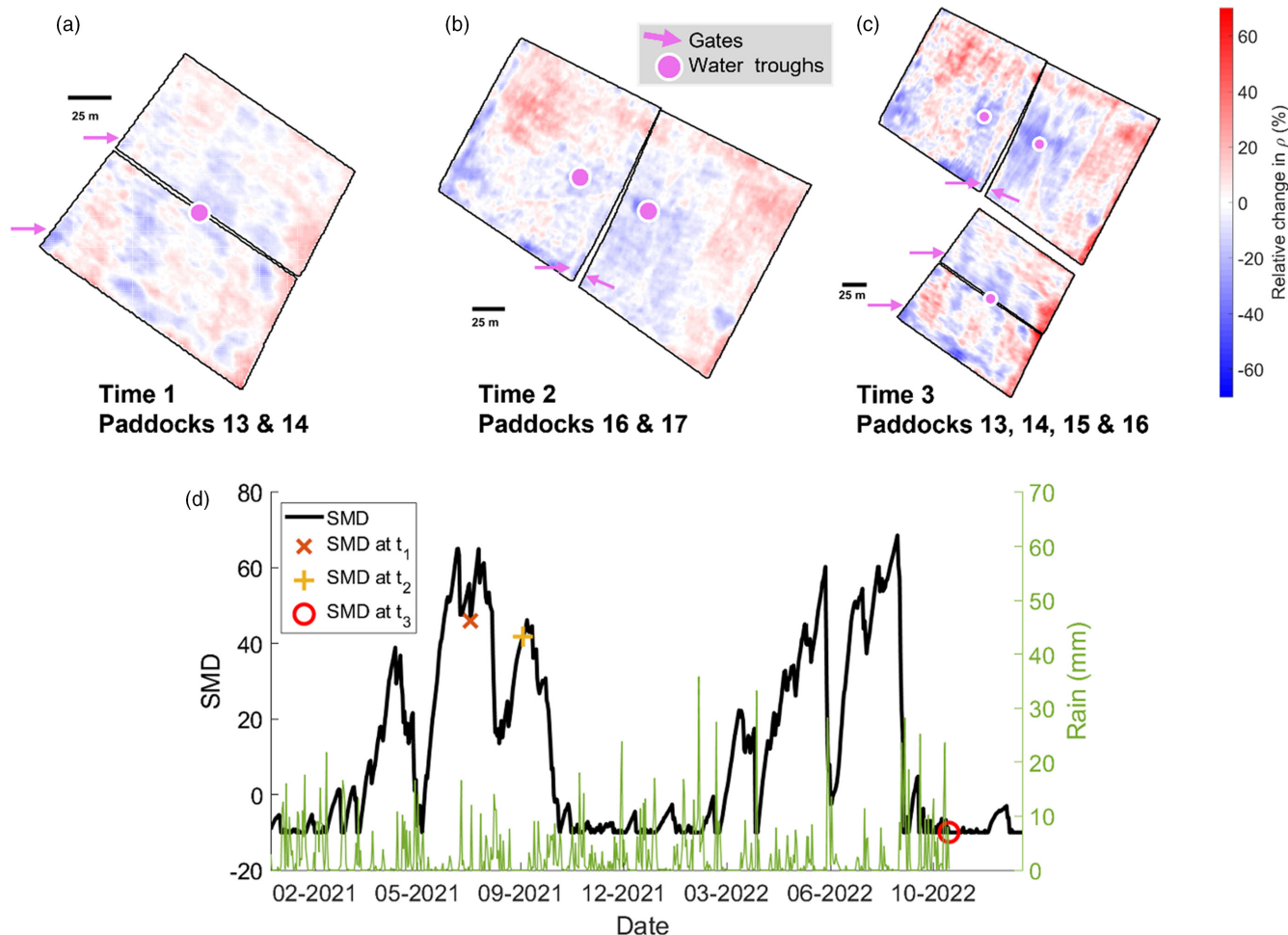
FIGURE 4 Within field relative changes in apparent electrical resistivity for electromagnetic induction data collected with a coil spacing of 0.33 m in (a) July 2021, (b) September 2021 and (c) October 2022. (d) Soil moisture deficit (SMD) calculated continuously for 2021 and 2022. SMD values for Times 1, 2 and 3 are marked in the figure.

patterns revealed by EMI data are consistent regardless of the soil moisture, temperature and time of the year. These spatial patterns are maintained in the relative apparent resistivity $\overline{\rho_a}$ calculated from data from all coil separations (see Figure S3). This is expected since data from larger coil separations sensitive to deeper soil depth ranges are still strongly affected by shallow soil depths (Figure 1d).

Regions with negative values of $\overline{\rho_a}$ are less electrically resistive than the mean resistivity of the paddock. Regions with positive values of $\overline{\rho_a}$ are more electrically resistive than the mean resistivity of the paddock. For all acquisition times, the areas with negative $\overline{\rho_a}$ coincide with the entry gates, the water troughs, and areas linking these two features of the paddock. In contrast, regions with higher $\overline{\rho_a}$ are most often those located the furthest away from the entry points. When comparing $\overline{\rho_a}$ between 2021 and 2022, approximately 10% of the area of all paddocks changed from negative to positive values. Similarly, approximately 10% of the areas changed from positive to negative values (Figure 5).

4.3 | Clustering

MCASD analysis (O'Leary et al., 2023), used for the first time here on EMI data, highlighted which number of clusters would be appropriate to define the EMI data acquired in these paddocks (see Figure S4). Three clusters per paddock/acquisition date were chosen for conceptual simplicity. The results from an increased number of clusters did not change the conclusions derived in this article (see Figure S5). The spatial structures resulting from clustering exhibit similar features for all paddocks regardless of the soil wetness conditions on the data collection date. The spatial structures in the cluster maps in Figure 6 correspond very well with the spatial structure of $\overline{\rho_a}$ maps shown in Figure 4. In addition, spatial patterns obtained in maps using data from 2021 are very similar to maps obtained with data from 2022, consistent with $\overline{\rho_a}$ results (Section 4.2).

Zones associated with the cluster centres having less resistivity values were near the locations of water troughs and entry gates where signs of compaction are visible and
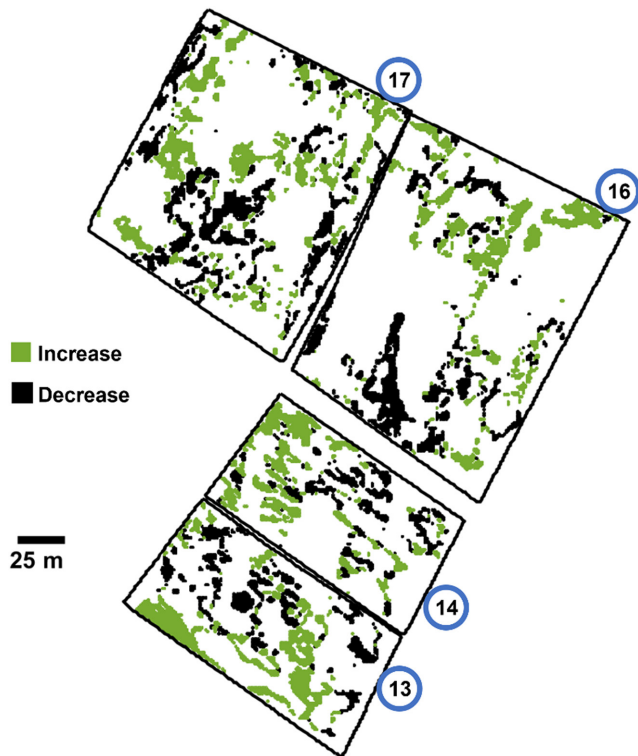
FIGURE 5 Map contrasting changes in relative apparent resistivity measured in 2021 and 2022. Regions changing from negative to positive values suggesting recovery are coloured in green. Regions changing from positive to negative values suggesting compaction are coloured in black.

expected. This is consistent with expectations for electrical properties of compacted soils. Based on this, we termed this zone as highly compacted soil. Since trampling (and hence compaction) occurs across the entire paddocks, zones associated with mid and high electrical resistivity cluster centres were termed moderately and low-compacted soils, respectively. These terms must be seen as relative and the values apply for this study only. Cluster centres corresponding for 0.33 m coil separation for all paddocks and times are reported in Table 1.

4.4 | Simulated apparent electrical resistivities

Figure 7 presents the modelling results of water contents of the first soil layer (0–0.23 cm) and the simulated apparent electrical resistivity for a coil separation of 0.33 cm (see sensitivity to soil depth in Figure 1d) for compacted and non-compacted soils from February 2021 to October 2022. Figure 7b shows the cluster centre values (Table 1) corresponding to low- and high-compacted zones for all paddocks and times. The simulated water contents show that the water contents are typically higher for compacted soils

than for non-compacted soils. During wet periods, both compacted and non-compacted soils have similar water contents, whereas on dry days non-compacted soil consistently become drier than compacted soils due to their ability to better drain water.

For both compacted and non-compacted soils, the modelled apparent electrical resistivities followed seasonal temperature trends and are very sensitive to variations of water contents. The pedophysical model of electrical resistivity was calibrated to reproduce data from Time 1 in the low compaction case in paddock 13. For this, the simulated apparent electrical resistivities successfully reproduced the clusters centres for Time 1 for both compacted and non-compacted soils. The simulated apparent electrical resistivities reproduced the cluster centres of Times 2 and 3 with a normalized root square mean (NRMS) of 1.2 (considering an error of 5%) and a correlation coefficient or $r = .96$. The simulated apparent resistivities are qualitatively consistent with the cluster observations and show good match between the simulated non-compacted and the measured low-compacted, and the simulated and measured highly compacted.

5 | DISCUSSION

5.1 | Signatures of grazing-induced compaction in EMI data

Our study constitutes an advance on soil compaction detection because it utilizes the flexibility of EMI to cover large areas. Clear spatial patterns were observed in both maps of $\overline{\rho_a}$ and cluster maps. The spatial patterns are present in all paddocks and on all acquisition days. The areas predicted to be compacted correspond very well with locations where compaction can be clearly identified with the naked eye (i.e., entry points and water troughs; see Figure 3c), and areas that are likely to be transited by animals (e.g., areas between gates and troughs). This suggests that long-term soil compaction produces primary signatures in the electrical resistivity data and that variations due to natural, within-field variations of soil texture may be less for the paddocks studied here. However, compaction may not be detectable in cases where the natural variations of soil texture are large and hence dominate spatial changes in soil electrical resistivity.

When comparing data from 2021 and 2022 (Figure 5), only 10% of the paddocks' areas changed from negative values in $\overline{\rho_a}$ to positive values. This may indicate post-compaction recovery of soil properties as commonly observed in grasslands (Drewry, 2006; Drewry et al., 2004). Despite this potential recovery, the same percentage of the paddocks' areas shifted from positive values of $\overline{\rho_a}$ to negative values, suggesting further compaction. This
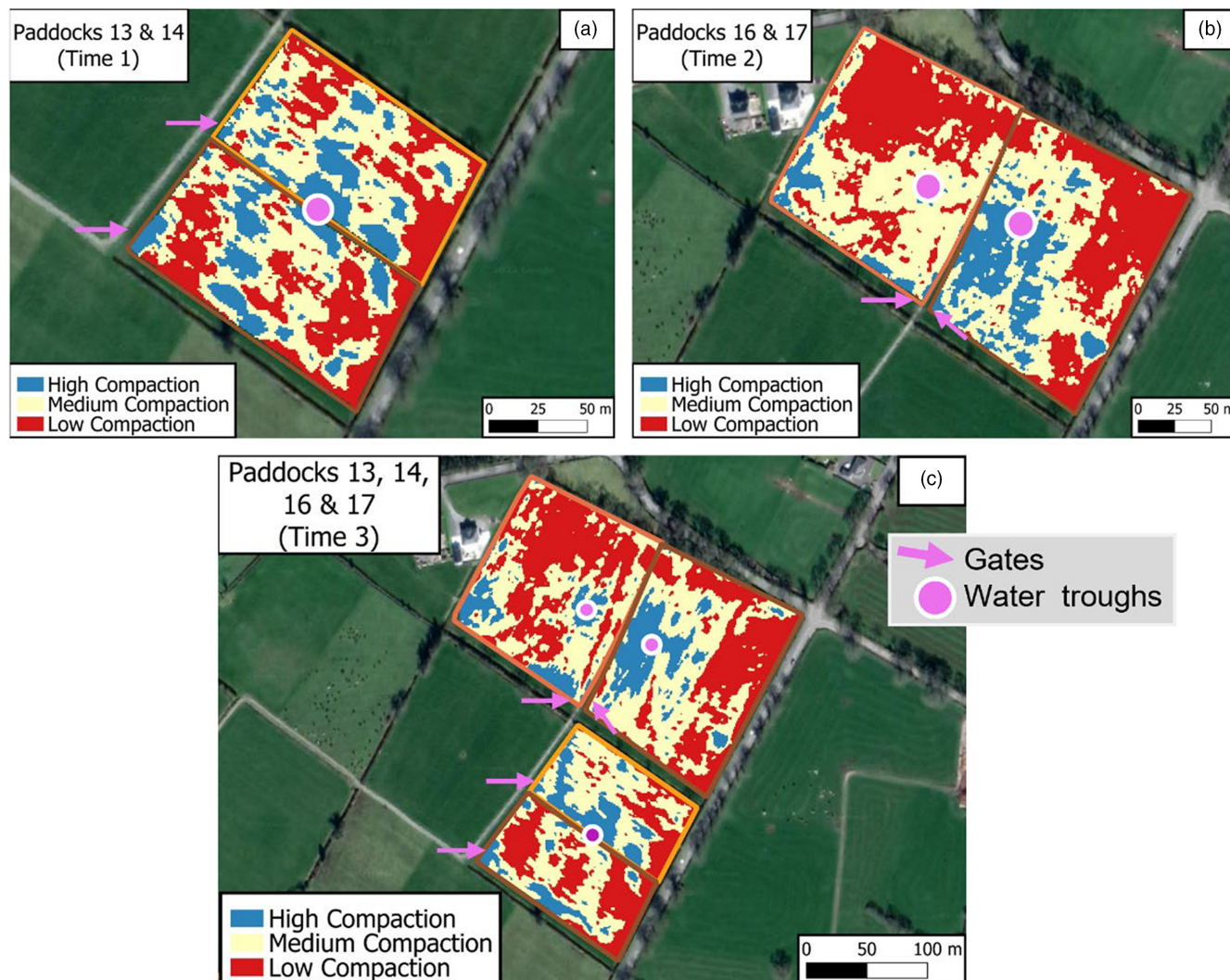
FIGURE 6 Spatial distribution of the three clusters derived using data from (a) July 2021, (b) September 2021 and (c) October 2022.

suggests that the grazing patterns of animals change randomly every year or that animals graze areas in one year that were less frequented the previous year, implying compaction related differences in grass yield. The areas of paddocks 16 and 17 is almost twice the areas of paddocks 13 and 14. In this farm, the paddocks are grazed under a rotational grazing strategy. The amount of time spent in the paddock will reflect (approximately) its size so larger paddocks will be split grazed using temporary fences and be subject to an overall longer residency time. Ultimately, a larger paddock (such as 16 and 17) supplies much more feed than a smaller paddock so is utilized as such to avoid undermining pasture quality and herd performance. This partly explains why paddocks 13 and 14 show similar values of apparent electrical resistivity in Time 3 (when measured simultaneously) and similar associated levels of compaction. This suggests that the rotationally grazing strategy effectively induces similar disturbance in soil structure for smaller and bigger paddocks. It is unclear, however, if this grazing strategy would be beneficial for

reducing the environmental impacts of grazing-induced soil compaction (e.g., increase in GHG emissions, see also Section 2) (De Klein et al., 2006). This requires further modelling, laboratory and field work and is outside the scope of this study.

5.2 | Clustering within paddock EMI data

Using an unsupervised machine learning algorithm, we identified three clusters in the EMI data that are associated with heavily, moderately and low-compacted soils. The clustering-based spatial delineation (Figure 6) led to very similar results from the relative difference-based areas (Figure 4) for identifying spatial patterns characteristics of soil compaction. The cluster centres output from the clustering algorithm allowed for EMI values to be assigned to each of these clusters which facilitated the link to predictive modelling results. When considering the cluster centres

TABLE 1 Apparent resistivity values of each cluster centre for each paddock/date acquisition. Only displaying the 0.33 m coil separation as this roughly relates to the depth where compaction is known to occur.

	Paddock 13	Paddock 14	Paddock 16	Paddock 17
Time 1 (16 July 2021)				
High compaction	88.67	89.04		
Medium compaction	101.93	97.71		
Low compaction	113.98	106.99		
Time 2 (03 September 2021)				
High compaction			105.32	87.94
Medium compaction			116.43	107.46
Low compaction			130.87	122.94
Time 3 (20 October 2022)				
High compaction	61.83	69.48	69.22	60.87
Medium compaction	76.52	80.96	81.83	74.26
Low compaction	92.52	95.91	96.26	87.74
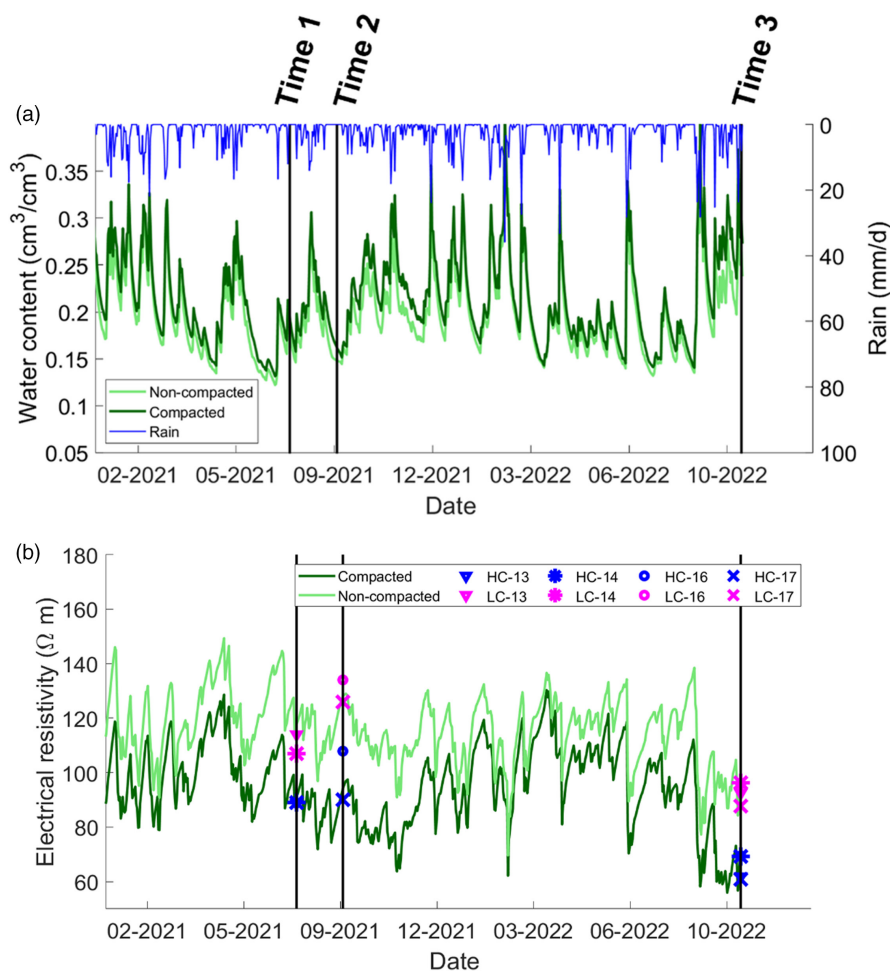
FIGURE 7 (a) Simulated water contents corresponding to the topsoil layer (0–23 cm) for non-compacted and compacted soils. (b) Simulated apparent electrical resistivity for non-compacted and compacted soils and cluster centres associated with low-compacted (LC) and high–compacted (HC) zones. Vertical black lines mark the dates in which electromagnetic induction data were collected.

associated with high compaction and low compaction, the decrease of apparent electrical resistivity (coil separation of 0.33 m) was 22%, 19% and 33% for Times 1, 2 and 3, respectively (See Table 1). When considering the cluster centres associated with high compaction and moderate compaction, the compaction-induced decrease of apparent

electrical resistivity was 12%, 9% and 19% for Times 1, 2 and 3, respectively. These differences are slightly higher, yet consistent, with the decrease in electrical resistivity observed in field studies using the ERT method in soils compacted by passages of agricultural machinery (Besson et al., 2004; Keller et al., 2017; Romero-Ruiz et al., 2022). Such slight

ROMERO-RUIZ ET AL.

Soil Use
and Management

BRITISH
SOCIETY
OF SOIL
SCIENCE

WILEY 13 of 16

differences with the literature values may be due to the different sensitivity to soil depth from the methods used, differences in soil type, compacting force, climate or compaction due to animal as opposed to machinery.

The clustering algorithm provided a powerful data-driven tool to reduce the dimensionality of the acquired data that focused this study on two specific scenarios to reproduce with agrogeophysical modelling. By comparing the measured decrease in apparent resistivities (see clusters centres in Figure 6b and Table 1), soil compaction effects were more evident on Time 3 (wet), followed by Time 1 (dry) and Time 2 (dry). This suggests that soil compaction effects on soil electrical properties are more evident on wet days, and thus, monitoring campaigns aimed at detection are more likely to be successful if performed on wet days, as recommended by Romero-Ruiz et al. (2022). However, it was still possible to clearly delineate the presumed compacted and non-compacted zones on Times 1 and 2, under dry conditions. In contrast, Romero-Ruiz et al. (2022) found that, in conditions when surface evaporation is important, compacted soils dried faster and more than non-compacted soils which masked compaction effects in the electrical resistivity. This is not observed in our study and may be also related to how the compaction mechanism (e.g., wheeling or trampling) changes soil hydrological and mechanical properties as a function of depth and time. Therefore, soil processes controlling soil water dynamics such as drainage, evaporation and root water uptake may be substantially different for each compaction type and likely depend on the climate too (through, e.g., differences in potential evapotranspiration). The observed increase in relative differences at Time 3 may be also driven by the fact that the paddocks had a higher number of total cumulative grazing days (since 2014) and seasonal grazing days (since the beginning of the grazing season in 2022).

5.3 | Agrogeophysical modelling: Limitations and outlook

Our newly developed agrogeophysical modelling approach allowed us to link aspects related to management such as grazing days and number of animals to soil electrical properties by considering the impact of management in soil processes. In such dynamic agricultural systems, these process-based modelling strategies have an advantage over traditional inversion of geophysical data that use smoothing constraints where infusing knowledge about the system is not straightforward (Tarantola, 2005). Despite the discrepancies between simulated and measured values of apparent electrical resistivities, the modelling results qualitatively confirmed the expectation and predicted decrease in the apparent electrical resistivity for the compacted soils. Since the model was calibrated using data from Time 1 in

the low-compacted paddock 13, the discrepancies between modelling results and observations can be associated with a combination of factors. The water flow module in the agro-ecosystem model may not be able to reproduce the moderately dry conditions in Time 1 and 2 and their differences fully, or the wet conditions expected for Time 3. This occurs in both compacted and low-compacted cases and thus may be caused by the simplifications in the choices of soil water retention and water flow properties that are the same in both systems. It is also likely that the simulated evaporation and root water uptake are overestimated. There may be other farm management practices which took place on Paddocks 16 and 17 that are not recorded in the grazing data provided (i.e., spraying and fertilizing) which may have affected the EMI results at Time 2. Finally, the differences may be related to the soil electrical properties defined for the compacted and non-compacted soils, which were simplified.

The modelling work is limited by its ability to represent soil properties and the soil processes associated with it. Despite these limitations, the model successfully reproduced the measured apparent resistivities to a NRMS of 0.98. As described in Section 2, mechanistic modelling work is important to help in understanding subsurface processes and harnessing monitoring techniques that allow quantification of such processes, the impact of soil management and to predict their environmental impacts (Vereecken et al., 2016).

The modelling approach presented here can be harnessed to use clustered EMI data in order to constrain spatially explicit models to help predicting field-scale impacts of grazing on soil functions due to compaction (e.g., increase in nitrous oxide emissions or reduction of carbon stocks) (Hu et al., 2021; Pulido-Moncada et al., 2022). This work offers the first attempt at linking a fully coupled model of soil management processes and its impact on geophysical signatures but further research is needed. Future work on developing a globally applicable modelling framework, requires more knowledge on the mechanistic links between management and geophysical data. This included a detailed field sampling campaign to acquire in situ soil data to constrain and validate the models presented here.

6 | CONCLUSIONS

We have developed a framework to model and detect the spatial extent of soil compaction in grasslands using field-scale EMI data. We measured EMI in paddocks of different sizes and under different soil wetness conditions in a dairy farm in Ireland. The EMI data were clustered using an unsupervised machine learning algorithm to obtain representative EMI signatures of spatial variation of soil

compaction. The clusters centres were then interpreted using a newly developed agrogeophysical modelling framework. The clustering results that were interpreted as compacted soils are consistent with field features such as water troughs and entry gates. Electrical resistivities measured for these zones are consistent with those reported for compacted soils in the literature. We suggest that, for these grasslands, compacted zones can be identified regardless of the size of the paddock and the soil wetness on the day of monitoring; however, this may be a characteristic that is unique to these climates and the nature of the compaction. The modelling framework presented here allowed us to mechanistically link measured field-scale EMI data with animal movement, soil compaction and a soil process model, which with further development may help to quantify, monitor and predict the field-scale and spatially explicit environmental consequences of different agricultural practices.

ACKNOWLEDGEMENTS

DATA AVAILABILITY STATEMENT

The data that support the findings of this study are available from the corresponding author upon reasonable request.

ORCID

Alejandro Romero-Ruiz https://orcid.org/0000-0002-6654-2908
Dave O'Leary https://orcid.org/0000-0002-4382-6115
Eve Daly https://orcid.org/0000-0002-4223-5129
Andrew P. Whitmore https://orcid.org/0000-0001-8984-1436

REFERENCES

Assouline, S., Narkis, K., Gherabli, R., Lefort, P., & Prat, M. (2014). Analysis of the impact of surface layer properties on evaporation from porous systems using column experiments and modified definition of characteristic length. *Water Resources Research*, *50*(5), 3933–3955.

Batey, T. (2009). Soil compaction and soil management – A review. *Soil Use and Management*, *25*(4), 335–345.

Benevenute, P. A. N., de Morais, E. G., Souza, A. A., Vasques, I. C. F., Cardoso, D. P., Sales, F. R., Severiano, E. C., Homem, B. G. C., Casagrande, D. R., & Silva, B. M. (2020). Penetration resistance: An effective indicator for monitoring soil compaction in pastures. *Ecological Indicators*, *117*, 106647.

Besson, A., Cousin, I., Samouëlian, A., Boizard, H., & Richard, G. (2004). Structural heterogeneity of the soil tilled layer as characterized by 2D electrical resistivity surveying. *Soil and Tillage Research*, *79*(2), 239–249.

Besson, A., Sger, M., Giot, G., & Cousin, I. (2013). Identifying the characteristic scales of soil structural recovery after compaction from three in-field methods of monitoring. *Geoderma*, *204*, 130–139.

Binley, A., Hubbard, S. S., Huisman, J. A., Revil, A., Robinson, D. A., Singha, K., & Slater, L. (2015). The emergence of hydrogeophysics for improved understanding of subsurface processes over multiple scales. *Water Resources Research*, *51*(6), 3837–3866.

Bondi, G., O'Sullivan, L., Fenton, O., Creamer, R., Marongiu, I., & Wall, D. P. (2021). Trafficking intensity index for soil compaction management in grasslands. *Soil Use and Management*, *37*(3), 504–518. https://doi.org/10.1111/sum.12586

Brogi, C., Huisman, J. A., Pätzold, S., von Hebel, C., Weihermüller, L., Kaufmann, M. S., van der Kruk, J., & Vereecken, H. (2019). Large-scale soil mapping using multi-configuration EMI and supervised image classification. *Geoderma*, *335*, 133–148.

Bussian, A. E. (1983). Electrical conductance in a porous medium. *Geophysics*, *48*(9), 1258–1268.

Campbell, R. B., Bower, C. A., & Richards, L. A. (1948). Change of electrical conductivity with temperature and the relation of osmotic pressure to electrical conductivity and ion concentration for soil extracts. *Soil Science Society of America Journal*, *13*, 66–69.

Carsel, R. F., & Parrish, R. S. (1988). Developing joint probability distributions of soil water retention characteristics. *Water Resources Research*, *24*(5), 755–769.

Carter, M. R. (1990). Relative measures of soil bulk density to characterize compaction in tillage studies on fine sandy loams. *Canadian Journal of Soil Science*, *70*(3), 425–433.

Coleman, K., Muhammed, S. E., Milne, A. E., Todman, L. C., Dailey, A. G., Glendining, M. J., & Whitmore, A. P. (2017). The landscape model: A model for exploring trade-offs between agricultural production and the environment. *Science of the Total Environment*, *609*, 1483–1499.

Creamer, R., & O'Sullivan, L. (2018). *The soils of Ireland*. Springer.

De Klein, C. A. M., Smith, L. C., & Monaghan, R. M. (2006). Restricted autumn grazing to reduce nitrous oxide emissions from dairy pastures in Southland, New Zealand. *Agriculture, Ecosystems \& Environment*, *112*(2–3), 192–199.

Drewry, J. J. (2006). Natural recovery of soil physical properties from treading damage of pastoral soils in New Zealand and

Australia: A review. *Agriculture, Ecosystems and Environment*, *114*(2–4), 159–169.

Drewry, J. J., Cameron, K. C., & Buchan, G. D. (2008). Pasture yield and soil physical property responses to soil compaction from treading and grazing—A review. *Soil Research*, *46*(3), 237–256.

Drewry, J. J., Paton, R. J., & Monaghan, R. M. (2004). Soil compaction and recovery cycle on a Southland dairy farm: Implications for soil monitoring. *Soil Research*, *42*(7), 851–856.

Durner, W. (1994). Hydraulic conductivity estimation for soils with heterogeneous pore structure. *Water Resources Research*, *30*(2), 211–223.

Farahani, E., Emami, H., & Keller, T. (2018). Impact of monovalent cations on soil structure. Part II. Results of two Swiss soils. *International Agrophysics*, *32*(1), 69–80.

Friedman, S. P. (2005). Soil properties influencing apparent electrical conductivity: A review. *Computers and Electronics in Agriculture*, *46*(1–3), 45–70.

Garré, S., Blanchy, G., Caterina, D., De Smedt, P., Romero-Ruiz, A., & Simon, N. (2022). Geophysical methods for soil applications. In *Reference module in earth systems and environmental sciences*. Elsevier. https://www.sciencedirect.com/science/article/pii/B978012822974300152X

Garré, S., Javaux, M., Vanderborght, J., Pags, L., & Vereecken, H. (2011). Three-dimensional electrical resistivity tomography to monitor root zone water dynamics. *Vadose Zone Journal*, *10*, 412–424. https://doi.org/10.2136/vzj2010.0079

Garré, S., Koestel, J., Gnther, T., Javaux, M., Vanderborght, J., & Vereecken, H. (2010). Comparison of heterogeneous transport processes observed with electrical resisvity tomography in two soils. *Vadose Zone Journal*, *9*(2), 336–349.

Ghezzehei, T. A., & Or, D. (2001). Rheological properties of wet soils and clays under steady and oscillatory stresses. *Soil Science Society of America Journal*, *65*(3), 624–637.

Hu, W., Drewry, J., Beare, M., Eger, A., & Mller, K. (2021). Compaction induced soil structural degradation affects productivity and environmental outcomes: A review and New Zealand case study. *Geoderma*, *395*, 115035.

Kaufman, L., & Rousseeuw, P. J. (2009). *Finding groups in data: An introduction to cluster analysis*. John Wiley & Sons.

Keller, T., Colombi, T., Ruiz, S., Manalili, M. P., Rek, J., Stadelmann, V., Wunderli, H., Breitenstein, D., Reiser, R., Oberholzer, H., Schymanski, S., Romero-Ruiz, A., Linde, N., Weisskopf, P., Walter, A., & Or, D. (2017). Long-term Soil Structure Observatory for monitoring post-compaction evolution of soil structure. *Vadose Zone Journal*, *16*(4), 1–16.

Keller, T., Lamande, M., Peth, S., Berli, M., Delenne, J., Baumgarten, W., Rabbel, W., & Radjaı, F. (2013). An interdisciplinary approach towards improved understanding of soil deformation during compaction. *Soil and Tillage Research*, *128*, 61–80.

Kohonen, T. (2013). Essentials of the self-organizing map. *Neural Networks*, *37*, 52–65.

Kowalsky, M. B., Finsterle, S., & Rubin, Y. (2004). Estimating flow parameter distributions using ground-penetrating radar and hydrological measurements during transient flow in the Vadose zone. *Advances in Water Resources*, *27*(6), 583–599.

Kuhl, A. S., Kendall, A. D., Dam, R. L. V., & Hyndman, D. W. (2018). Quantifying soil water and root dynamics using a coupled hydrogeophysical inversion. *Vadose Zone Journal*, *17*(1), 1–13.

Linde, N., Binley, A., Tryggvason, A., Pedersen, L. B., & Revil, A. (2006). Improved hydrogeophysical characterization using joint inversion of cross-hole electrical resistance and ground-penetrating radar traveltime data. *Water Resources Research*, *42*(12), W12404.

Lipiec, J. (2000). A review of the usefulness of relative bulk density values in studies of soil structure and compaction. *Soil & Tillage Research*, *53*, 71–85.

McLachlan, P., Blanchy, G., & Binley, A. (2021). EMagPy: Open-source standalone software for processing, forward modeling and inversion of electromagnetic induction data. *Computers & Geosciences*, *146*, 104561.

Meurer, K., Barron, J., Chenu, C., Coucheney, E., Fielding, M., Hallett, P., Herrmann, A. M., Keller, T., Koestel, J., Larsbo, M., Lewan, E., Or, D., Parsons, D., Parvin, N., Taylor, A., Vereecken, H., & Jarvis, N. (2020). A framework for modelling soil structure dynamics induced by biological activity. *Global Change Biology*, *26*(10), 5382–5403.

Minsley, B. J., Smith, B. D., Hammack, R., Sams, J. I., & Veloski, G. (2012). Calibration and filtering strategies for frequency domain electromagnetic data. *Journal of Applied Geophysics*, *80*, 56–66.

O'Leary, D., Brown, C., Healy, M. G., Regan, S., & Daly, E. (2023). Observations of intra-peatland variability using multiple spatially coincident remotely sensed data sources and machine learning. *Geoderma*, *430*, 116348.

Or, D., Keller, T., & Schlesinger, W. H. (2021). Natural and managed soil structure: On the fragile scaffolding for soil functioning. *Soil and Tillage Research*, *208*, 104912.

Pulido-Moncada, M., Petersen, S. O., & Munkholm, L. J. (2022). Soil compaction raises nitrous oxide emissions in managed agroecosystems. A review. *Agronomy for Sustainable Development*, *42*(3), 1–26.

Rabot, E., Wiesmeier, M., Schlter, S., & Vogel, H. (2018). Soil structure as an indicator of soil functions: A review. *Geoderma*, *314*, 122–137.

Rivero, M. J., Grau-Campanario, P., Mullan, S., Held, S. D. E., Stokes, J. E., Lee, M. R. F., & Cardenas, L. M. (2021). Factors affecting site use preference of grazing cattle studied from 2000 to 2020 through GPS tracking: A review. *Sensors*, *21*(8), 2696.

Romero-Ruiz, A., Linde, N., Baron, L., Breitenstein, D., Keller, T., & Or, D. (2022). Lasting effects of soil compaction on soil water regime confirmed by geoelectrical monitoring. *Water Resources Research*, *58*(2), e2021WR030696.

Romero-Ruiz, A., Linde, N., Keller, T., & Or, D. (2018). A review of geophysical methods for soil structure characterization. *Reviews of Geophysics*, *56*(4), 672–697.

Romero-Ruiz, A., Milne, A., Meo-Filho, P. D., Pulley, S., Segura, C., Rivero-Viera, J., Coleman, K., Cardenas, L., & Whitmore, A. (2023). Grazing livestock move by Lévy walks: Implications for soil health and environment. *Journal of Environmental Management*, *345*, 118835.

Romero-Ruiz, A., Monaghan, R., Milne, A., Coleman, K., Cardenas, L., Carmen, S., & Whitmore, A. (2023). Modelling changes in soil structure caused by livestock treading. *Geoderma*, *431*, 116331. https://doi.org/10.1016/j.geoderma.2023.116331

Schmäck, J., Weihermüller, L., Klotzsche, A., von Hebel, C., Pätzold, S., Welp, G., & Vereecken, H. (2022). Large-scale detection and quantification of harmful soil compaction in a post-mining landscape using multi-configuration electromagnetic induction. *Soil Use and Management*, *38*(1), 212–228. https://doi.org/10.1111/sum.12763

Schulte, R. P. O., Diamond, J., Finkele, K., Holden, N. M., & Brereton, A. J. (2005). Predicting the soil moisture conditions of Irish grasslands. *Irish Journal of Agricultural and Food Research*, *44*, 95–110.

Seladji, S., Cosenza, P., Tabbagh, A., Ranger, J., & Richard, G. (2010). The effect of compaction on soil electrical resistivity: A laboratory investigation. *European Journal of Soil Science*, *61*(6), 1043–1055.

Sen, P. N., Scala, C., & Cohen, M. H. (1981). A self-similar model for sedimentary rocks with application to the dielectric constant of fused glass beads. *Geophysics*, *46*(5), 781–795. https://doi.org/10.1190/1.1441215

Steinfeld, H., Gerber, P., Wassenaar, T. D., Castel, V., Rosales, M., Rosales, M., & de Haan, C. (2006). *Livestock's long shadow: Environmental issues and options*. Food & Agriculture Organization.

Stephenson, M. B., & Bailey, D. W. (2017). Do movement patterns of GPS-tracked cattle on extensive rangelands suggest independence among individuals? *Agriculture*, *7*(7), 58.

Tarantola, A. (2005). *Inverse problem theory and methods for model parameter estimation*. Society for industrial and applied mathematics.

Tuohy, P., Fenton, O., Holden, N. M., & Humphreys, J. (2015). The effects of treading by two breeds of dairy cow with different live weights on soil physical properties, poaching damage and herbage production on a poorly drained clay-loam soil. *The Journal of Agricultural Science*, *153*(8), 1424–1436.

Vereecken, H., Schnepf, A., Hopmans, J. W., Javaux, M., Or, D., Roose, T., Vanderborght, J., Young, M., Amelung, W., Aitkenhead, M., Allison, S. D., Assouline, S., Baveye, P., Berli, M., Brggemann, N., Finke, P., Flury, M., Gaiser, T., Govers, G., … Lamorski, K. (2016). Modeling soil processes: Review, key challenges and new perspectives. *Vadose Zone Journal*, *15*(5), 1–57.

von Hebel, C., Reynaert, S., Pauly, K., Janssens, P., Piccard, I., Vanderborght, J., van der Kruk, J., Vereecken, H., & Garré, S. (2020). Toward high-resolution agronomic soil information and management zones delineated by ground-based electromagnetic induction and aerial drone data. *Vadose Zone Journal*, *20*, e20099.

von Hebel, C., Rudolph, S., Mester, A., Huisman, J. A., Kumbhar, P., Vereecken, H., & van der Kruk, J. (2014). Three-dimensional imaging of subsurface structural patterns using quantitative large-scale multiconfiguration electromagnetic induction data. *Water Resources Research*, *50*(3), 2732–2748. https://doi.org/10.1002/2013WR014864

Waxman, M. H., & Smits, L. J. M. (1968). Electrical conductivities in oil-bearing Shaly sands. *Society of Petroleum Engineers Journal*, *8*(2), 107–122.

SUPPORTING INFORMATION

Additional supporting information can be found online in the Supporting Information section at the end of this article.

How to cite this article: Romero-Ruiz, A., O'Leary, D., Daly, E., Tuohy, P., Milne, A., Coleman, K., & Whitmore, A. P. (2024). An agrogeophysical modelling framework for the detection of soil compaction spatial variability due to grazing using field-scale electromagnetic induction data. *Soil Use and Management*, *40*, e13039. https://doi.org/10.1111/sum.13039